European Annals of Otorhinolaryngology, Head and Neck diseases 136 (2019) 87–92

Available online at
ScienceDirect
www.sciencedirect.com

Elsevier Masson France
EM|consulte
www.em-consulte.com/en

Original article

Computational Fluid Dynamics in the assessment of nasal obstruction in children

E. Moreddu[a,b,*], L. Meister[a], C. Philip-Alliez[a], J.-M. Triglia[b], M. Medale[a], R. Nicollas[a,b]

[a] IUSTI, UMR 7343, CNRS, Aix-Marseille university, 13005 Marseille, France
[b] Department of pediatric otolaryngology, Aix-Marseille university, La Timone Children's hospital, 13005 Marseille, France

ARTICLE INFO

Keywords:
Nasal obstruction
Computational fluid dynamics
Rhinomanometry
Children
Pediatrics

ABSTRACT

Objectives: Nasal obstruction is a highly subjective symptom. It can be evaluated by combining clinical examination, imaging and functional measurements such as active anterior rhinomanometry (AAR). In pediatrics, AAR is often impossible because it requires the participation of the child. Airflow modeling by Computational Fluid Dynamics (CFD) has been developed since the early 1990s, mostly in adults. This study is the first to describe a methodology of "numerical rhinomanometry" in children using CFD and to evaluate the feasibility and the clinical interest of this new tool.
Materials and methods: Five children aged from 8 to 15 years, complaining of nasal obstruction, underwent routine management including clinical evaluation, AAR, and CT-scanning. CT acquisitions were used for CFD calculations and numerical rhinomanometry.
Results and conclusions: In the 5 children, the results of CFD were concordant with clinical complaints and examination. In 3 children, AAR and CFD were concordant. In one patient, CFD corrected the results of AAR. In one patient, AAR was not feasible, unlike CFD, which contributed to diagnosis. This study highlighted the feasibility of CFD in children and that it can support or refute diagnosis of nasal obstruction with good reliability. These results indicate that CFD modeling could be widely used for functional exploration in pediatric rhinology.

1. Introduction

The physiology of nasal breathing is closely related to fluid mechanics in humans. Changes in the normal anatomy of the nasal fossae can modify airflow and lead to disorders such as nasal obstruction. In children, chronic nasal obstruction is a common problem that may affect sleep and facial growth [1,2]. The treatment of these breathing disorders sometimes requires a surgical correction of the nasal fossae to normalize airflow.

Nasal obstruction is a highly subjective symptom, and otolaryngologists have long been interested in techniques providing objective evaluations [3]. In pediatric rhinology, one of these commonly used objective assessments is the measurement of nasal resistances with Active Anterior Rhinomanometry (AAR). AAR provides pressure-flow curves and resistance values that can be easily used in clinical practice [4]. In some cases, there is a lack of correlation between reported symptoms and objective findings [5–8]. In other cases, AAR is impractical because it requires the active participation of the child, which can rarely be relied upon before 5 years of age [9].

The use of numerical modeling, particularly airflow modeling with Computational Fluid Dynamics (CFD) [10], has become an important area of research in the past few years. The pioneer studies in the 1990s [11,12] oversimplified the geometry of the nasal cavities and were limited to a single side. With the improvement of computing power, 3D reconstructions of nasal cavities became more accurate and complex airflow patterns were discovered in the nasal fossae [13–17]. Nasal abnormalities have been more frequently described using numerical simulations, such as empty-nose syndrome or septal deviations [18–20]. Some authors recommend virtual surgical planning using CFD models [21–23].

Most of the previous studies used a simplified 3D geometry of the nasal airway and the RANS (Reynolds Averaged Navier-Stokes) methodology providing information about steady-state flow through the nose [24]. Unsteady-state calculations are more time-consuming, but provide mass flows and pressure values over time and allow a "numerical rhinomanometry". The interest of CFD in the evaluation of nasal obstruction has never been evaluated

* Corresponding author at: Department of pediatric otolaryngology, Aix-Marseille university, La Timone Children's hospital, 264, rue Saint-Pierre, 13005 Marseille, France.
E-mail address: eric.moreddu@ap-hm.fr (E. Moreddu).

https://doi.org/10.1016/j.anorl.2018.11.008
1879-7296/

in children, despite its potential contribution in surgical decision-making in selected cases. It can be easily compared to AAR, which is the gold-standard examination for flow-pressure curves and nasal resistance evaluation. Moreover, the feasibility and significance of numerical models of nasal airflow have not yet been evaluated in pediatric populations.

The objectives of the present work are to describe the methodology to create a numerical rhinomanometry in a pediatric population, based on unsteady-state CFD calculations, and also to evaluate the clinical interest of this numerical tool to improve the diagnosis of nasal obstruction in children.

2. Materials and methods

Five patients were included in the study. In line with French regulations, informed consent was obtained from the parents or legal representative and from the child at each step. According to article L. 1121-1 of the French Public Health Code, review board approval was not needed for this kind of research, which did not affect usual management. The study was conducted in accordance with the Declaration of Helsinki and French Good Clinical Practices. Patients underwent clinical examination, AAR and CT-scanning. CT was used for CFD calculation and to create the numerical rhinomanometry. The results of these examinations were then compared.

2.1. Anterior active rhinomanometry

AAR (Rhinomanometer NR6; GM Instruments Ltd.) was performed on all subjects according to the recommendations of the Standardization Committee. The acquisitions were performed less than 30 minutes after CT-scanning to avoid changes linked with the nasal cycle. No medication, including local vasoconstrictors, was used. Four consecutive respiratory cycles were recorded and mean unilateral nasal airway resistance values were used for calculations. Nasal resistance was calculated as $\Delta p/Q$, where Δp is the pressure drop in Pascals (Pa) between the nostrils and posterior nose, and Q is the flow rate in milliliters per second (ml/s). Results were reported as mean values on the four nasal cycles.

2.2. CT acquisition

CT indications were based on our usual protocol. Patients were selected as showing chronic nasal obstruction requiring CT. In our usual practice, CT-scanning is performed prior to surgery, in the Pediatric Radiology Department of our institution, with the following properties: acquisition matrix of 512*512 pixels, pixel size of 0.3*0.6 mm and voxel depth of 0.8 mm. The DICOM stack acquired from the CT-scan was then used for 3D reconstruction.

2.3. Computational fluid dynamics

Numerical simulations of airflows were performed using computational fluid dynamics (CFD). These simulations are based on the numerical solution of the Navier–Stokes equation, which is a general equation for three-dimensional flow of compressible and viscous (Newtonian) fluids. A segregated flow model with a second-order convective scheme was used for the resolution of the Navier–Stokes equation. Three major steps are required for the simulations:

- construction of a geometrical model from CT data;
- assignment of the discrete computational domain into computational cells (known as discretization), resulting in the generation of a computational mesh;
- and solution of the conservation equations on this mesh until a numerically convergent solution is obtained.

3D reconstruction of the nasal fossae from CT imaging was performed using image segmentation software (ITK-SNAP®, University of Pennsylvania, Philadelphia, PA). As the geometry of normal and pathologic nasal fossae is very complex, this step was one the most critical for our study. In order to virtually isolate the nasal fossae from adjacent regions, and reconstruct its entire volume, semi-automatic threshold-based segmentation with manual corrections was carried out using the half-maximum height method [25], which is a thresholding protocol for the region of interest [26], and by taking repeated measurements in 20 different zones of the virtual stack [27] using the ITK-Snap and ImageJ v.1.45s software packages. The segmented geometries were exported as Standard Tessellation Language (STL) files into the STAR-CCM+® (CD-Adapco) CFD code used to simulate airflow. Depending on nasal fossa anatomy, meshes with an order of magnitude of 5 million computational cells were generated.

Unsteady-state inspiratory airflow simulations were performed on Star-CCM+® software using two representative respiratory cycles previously acquired as mean values from 20 healthy subjects. The boundary conditions used to determine the airflow field were set as follows: “wall” condition of zero parietal velocity assuming and undeformable non-sliding airway wall, relative “inlet” pressure condition at the nostrils with gauge pressure set to 0, and relative “outlet” pressure condition with gauge pressure set to variable negative values according to the nasal cycle. The gas used in our simulation was air, with the following physical properties: external room temperature, 19 °C; ambient atmospheric pressure, 1013.25 hPa; density, $\rho_{air} = 1.161\ kg/m^3$; and dynamic viscosity $\mu_{air} = 1.8 \times 10^{-5}\ kg/m^{-1}s^{-1}$. Pressure drop values were computed by averaging total inlet and outlet pressures.

CFD outcome measures included nasal pressure and flow within the nasal cavity. Nasal resistances were calculated as $\Delta p/Q$, where Δp is the pressure difference in Pascals (Pa) between the nostrils and posterior end of the cavity, and Q is the flow rate in milliliters per second (ml/s). Data were exported to a Table showing time and pressure according to time, and converted into flow/pressure curves using GnuPlot® software, thus creating a numerical rhinomanometry.

3. Results

Five patients were included in this study. Age range was 8 to 15 years. Absolute resistance values on AAR and CFD are shown in Table 1. Total resistance (TR), right fossa resistance (RR) and left fossa resistance (LR) at 150 Pa/s were analyzed for each patient.

3.1. Case #1

A 9-year old male presented with chronic nasal obstruction. The clinical examination revealed posterior leftward

Table 1
Comparison of AAR and CFD results.

Patient	Total resistance ($Pa.s.m^{-3}$)		Right resistance ($Pa.s.m^{-3}$)		Left resistance ($Pa.s.m^{-3}$)	
	AAR	CFD	AAR	CFD	AAR	CFD
1	0.45	0.34	0.56	0.4	2.2	2.2
2	0.52	0.24	1.07	0.42	1.04	0.53
3	0.35	0.26	1.04	0.62	0.53	0.47
4	0.24	0.22	0.58	0.64	0.41	0.35
5		0.17		0.34		0.37

AAR: active anterior rhinomanometry; CFD: computational fluid dynamics.

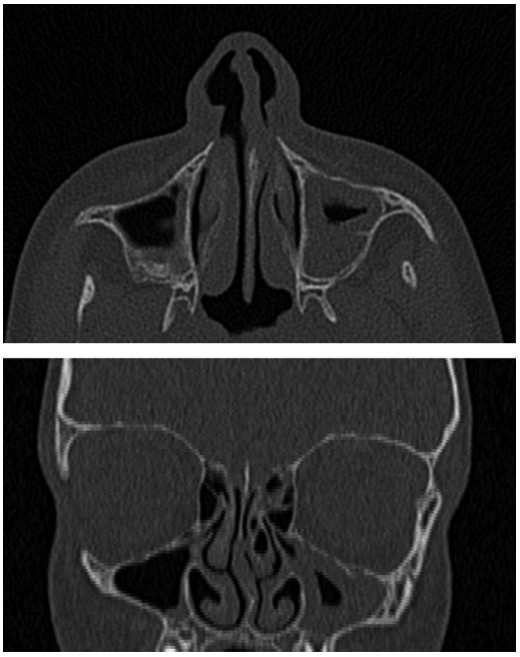

Fig. 1. Axial (upper part of the figure) and coronal (lower part of the figure) CT slices of in case #1, showing leftward septal deviation and inferior turbinate hypertrophy.

septal deviation and bilateral inferior turbinate hypertrophy with left-sided predominance. CT confirmed the septal deviation and inferior turbinate hypertrophy (Fig. 1). The AAR measured slightly elevated total resistance with severe left nasal obstruction (TR = 0.45 Pa/ml/s, RR = 0.56 Pa/ml/s, LR = 2.20 Pa/ml/s). CFD confirmed severe pressure loss, higher velocity and lower airflow in the left nasal fossa (TR = 0.34 Pa/ml/s, RR = 0.4 Pa/ml/s, LR = 2.20 Pa/ml/s). CFD was thus concordant to AAR, with decreased left nasal permeability (Fig. 2). In this case, clinical examination, CT, AAR and CFD were all concordant. The slightly elevated global resistance measured on AAR and CFD masked severe left nasal obstruction. This patient underwent septoplasty with bilateral laser cauterization of the inferior turbinates, with subsequent normalization of nasal breathing and resistances on AAR, at 22 months' follow-up.

3.2. Case #2

A 15-year old female presented with moderate nasal obstruction. Clinical examination revealed bilateral inferior turbinate hypertrophy, without septal deviation. CT showed bilateral inferior turbinate hypertrophy and right concha bullosa. The AAR showed high total resistance, with high resistance in both nasal fossae (TR = 0.52 Pa/ml/s, RR = 1.04 Pa/ml/s, LR = 1.02 Pa/ml/s). CFD found subnormal resistance, with a slight difference between the two fossae, with greater pressure loss, higher velocity and lower flow in the left fossa (TR = 0.24 Pa/ml/s, RR = 0.53 Pa/ml/s, LR = 0.42 Pa/ml/s) (Fig. 2). In this case, there was a close correlation between the history taking and CFD, whereas AAR appeared to overestimate nasal airway resistance. Medical treatment associating nasal saline wash and nasocorticoids was first proposed. After initial improvement, inferior turbinoplasty was performed six months later due to recurrence of nasal obstruction with high nasal resistance on AAR, not improved by decongestants. Nasal breathing and resistances were obtained, at 14 months' follow-up.

3.3. Case #3

An 8-year old male presented with nasal obstruction. Clinical examination revealed severe rightward anterior septal deviation, preventing flexible endoscopy. CT confirmed anterior septal deviation blocking the right nasal fossa. AAR showed slightly elevated total resistance, 2-fold greater in the right fossa (TR = 0.35 Pa/ml/s, RR = 1.04 Pa/ml/s, LR = 0.53 Pa/ml/s). CFD identified higher-pressure loss in the right fossa (TR = 0.26 Pa/ml/s, RR = 0.62 Pa/ml/s, LR = 0.47 Pa/ml/s) (Fig. 2). In this case, interview, CT, AAR and CFD were concordant. The child underwent septoplasty. Normal nasal breathing and resistances were obtained, at 26 months' follow-up.

3.4. Case #4

A 13-year old male was referred by his orthodontist for exclusive oral breathing without complaint of nasal obstruction. Clinical examination and CT revealed bilateral inferior turbinate hypertrophy predominantly in the right nasal fossa associated with an architectural abnormality of the bony palate. AAR (TR = 0.24 Pa/ml/s, RR = 0.58 Pa/ml/s, LR = 0.41 Pa/ml/s) and CFD (TR = 0.22 Pa/ml/s, RR = 0.64 Pa/ml/s, LR = 0.35 Pa/ml/s) did not identify any nasal obstruction, though airflow was 30% higher in the left than the right nasal fossa. CFD was concordant with clinical examination and AAR (Fig. 2). In this case, all modes of evaluation of nasal permeability ruled out nasal etiology for exclusive oral breathing. Orthodontic treatment with palatal expansion was deemed more appropriate than nasal surgery. Normal nasal breathing and resistances on AAR were obtained, at 23 months' follow-up.

3.5. Case #5

A 14-year old male presented with mixed oral and nasal ventilation and suspicion of nasal obstruction. Clinical examination and CT were normal and symmetric. AAR could not be performed as the patient was unable to breathe through the mask; CFD was thus the sole means of assessing airway permeability (TR = 0.17 Pa/ml/s, RR = 0.34 Pa/ml/s, LR = 0.37 Pa/ml/s): numerical rhinomanometry confirmed normal symmetric flow/pressure curves (Fig. 2). As a result, the patient did not undergo any surgical or medical treatment, but rather of nasal breathing rehabilitation. Normal nasal breathing and resistances on AAR were obtained, at 1 year's follow-up.

4. Discussion

This study is, to our knowledge, the first to describe the process of the creation of numerical rhinomanometry using CFD techniques. We demonstrated that 3D reconstruction of pediatric nasal fossae is possible, and that CFD with unsteady-state calculations can support or refute diagnosis of nasal obstruction with good reliability, when compared to AAR.

In the five children, the results of numerical rhinomanometry by CFD were concordant with clinical complaints and examinations. In three cases (cases #1, 3 and 4), the results of CFD were concordant with clinical complaints and with AAR. In one case (case #2), AAR overestimated nasal resistance compared to patient's complaint, whereas CFD was initially concordant with both clinical evaluation and the patient's complaint; the patient finally underwent surgical intervention due to recurrence of nasal obstruction after initial improvement. This illustrates the fact that nasal resistances may change over time and assessment should be repeated according to the patient's complaints. Case #3 highlighted the fact that in patients with asymmetric fossae, total resistance is not relevant in evaluating the severity of nasal obstruction. In one case

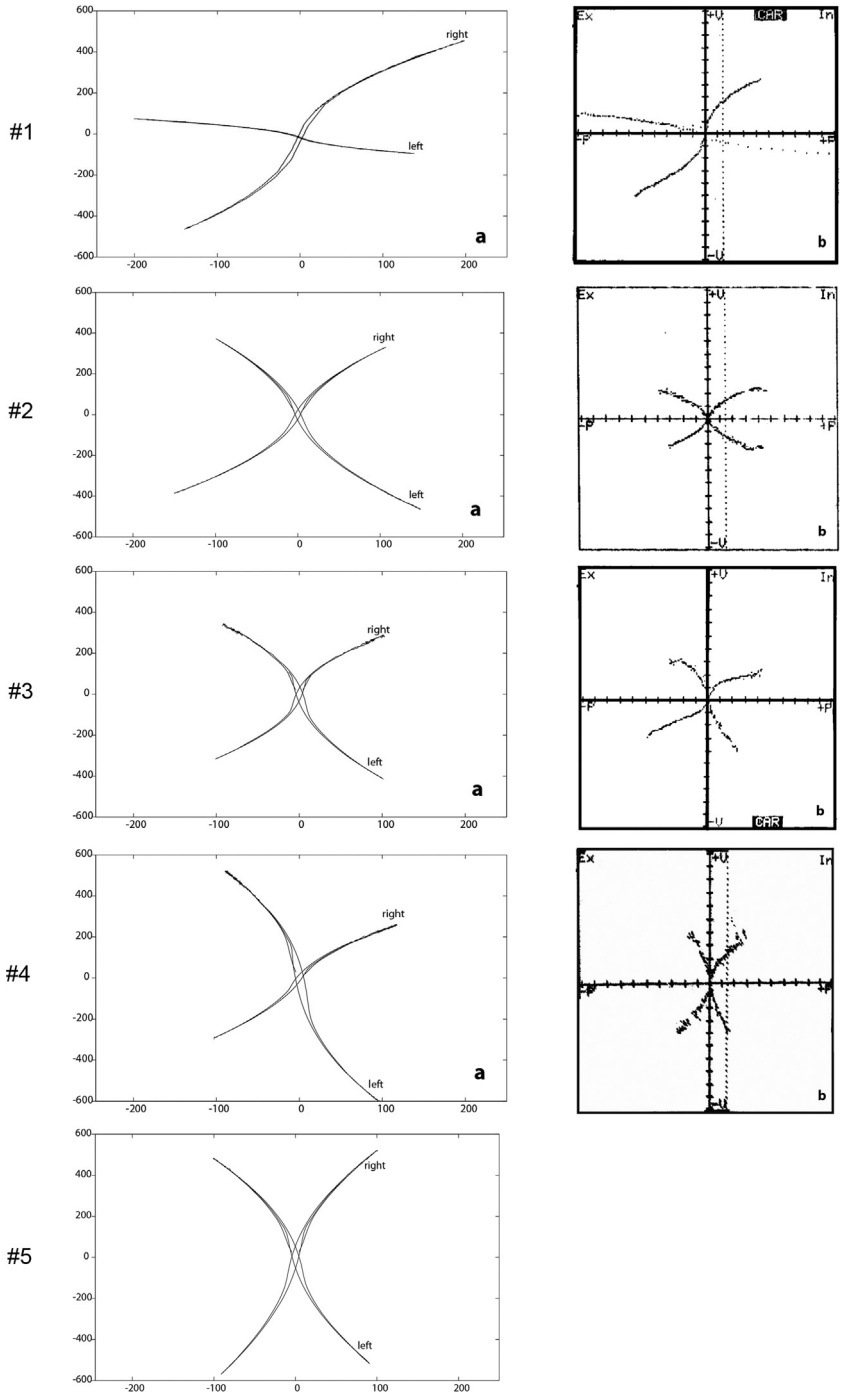

Fig. 2. Comparison between curves for all patients. CFD curves are shown on the left (a) and AAR curves on the right (b). For case #5, only CFD curves were available.

(case #5), AAR was not initially feasible and CFD was helpful for diagnosis; normal CFD curves were confirmed when AAR became feasible after 1 year's rehabilitation of nasal breathing. In this case, the perfect symmetry found between the two nasal fossae may be explained either by lack of nasal cycle, as in about 20% of the general population, and/or the timing of the CT scan at nasal cycle inversion. We think that CFD may also identify anomalies not detected by AAR, such as anterior obstruction, where inserting the sensor modifies local anatomy. CFD can also clarify the diagnosis of nasal obstruction when CT-scan and AAR are discordant, especially in defective AAR acquisition. However, in the present protocol, CT was performed before initiation of vasoconstrictors, and was not repeated, to avoid excessive X-ray exposure; thus CFD could not anticipate the results of treatment of mucosal nasal obstruction, contrary to AAR with decongestants. CFD-simulated values are approximations to real conditions, depending only on nasal geometry; they should not be taken as directly representing real conditions. However, the qualitative aspect of the curves and the relative differences between the two sides are interesting to analyze.

AAR is a frequently-used functional assessment of nasal ventilation. AAR measures variations in global pressure and flow during

four respiratory cycles in each nasal fossa, and calculates nasal resistances. These values can also be simulated on CFD: AAR can thus be used as a gold-standard to assess CFD reliability. Other functional evaluations exist, but do not provide the information directly correlating with numerical simulations. AAR is quick, easy to perform and provides additional information that is beneficial in many cases. In combination with vasoconstrictors, AAR may identify the cause of obstruction as being either structural or mucosal, but cannot precisely identify the site of the obstruction [8]. AAR may also refute nasal obstruction when no abnormalities of flow or pressure are observed, such as in empty-nose syndrome. Although AAR has been extensively studied, one of its major limitations is a lack of correlation between patient's complaints and objective measurements [5–8]. Some children present indirect signs of nasal obstruction without voicing their symptoms, while others complain of nasal obstruction without having identifiable abnormalities on imaging and functional studies [3]. Technical problems that may distort the accuracy of AAR include: poor calibration of the rhinomanometer, oral breathing, deformity of the first third of the nasal fossae by the sensor, or leak around the ventilation mask. Finally, AAR is restricted to children who are able to cooperate and follow instructions, usually after 5 years of age.

Building CFD models necessitates CT acquisition. The main limitation of numerical modeling of airway permeability in children is thus X-ray exposure. In this study, all patients underwent CT as part of routine clinical management, to confirm diagnosis and perform preoperative planning for chronic nasal obstruction. The CT technique was not modified for research purposes, with the usual radiation dose. Due to this limitation, CFD techniques cannot be generalized to all patients, and should be performed only when clinical and functional assessments do not provide sufficient information decision-making, and when CT is contributive.

In these selected cases, CT 3D reconstruction of the nasal fossae is the critical step. Thresholding to locate the nasal fossae walls can be manual or semi-automated. The semi-automated method using the half-maximum height (HMH) threshold is less subjective [26], but manual operations are unfortunately still required, especially in case of nasal fossa secretions that may lead to inaccurate semi-automated reconstruction. Once the 3D-reconstruction achieved, CFD unsteady-state calculations and post-treatment are time-consuming and require several days. This is presently a limitation to the use of CFD, but the time needed should decrease with increasing computing power. It should also be borne in mind that CFD models are based on theoretical boundary conditions, giving results that are approximations of the true conditions, and faithful only to nasal geometry.

5. Conclusion

CFD is a promising method for studying chronic nasal obstruction in children. This study demonstrated its feasibility and reliability in a pediatric population. Unsteady-state calculations hold great potential for evaluating the quality of nasal airflow and can provide dynamic pressure/flow curves close to those obtained with AAR. In selected cases, CFD can rectify AAR or replace it. In the future, with automation of the procedure, on which we are presently working, and increased computing power, CFD may become a widespread tool in surgical decision-making and prediction of surgical results. Our results encourage us to continue modeling nasal airflow and to study airflow in pathologic conditions using CFD.

Ethical statement

Ethical approval: All procedures performed in studies involving human participants were in accordance with the ethical standards of the institutional and/or national research committee and with the 1964 Helsinki Declaration and its later amendments or comparable ethical standards.

Informed consent: Informed consent was obtained from all individual participants included in the study.

Disclosure of interest

The authors declare that they have no competing interest.

References

[1] D'Ascanio L, Lancione C, Pompa G, Rebuffini E, Mansi N, Manzini M. Craniofacial growth in children with nasal septum deviation: a cephalometric comparative study. Int J Pediatr Otorhinolaryngol 2010;74:1180–3.
[2] Sullivan S, Li K, Guilleminault C. Nasal obstruction in children with sleep-disordered breathing. Ann Acad Med Singapore 2008;37:645–8.
[3] Occasi F, Duse M, Vittori T, et al. Primary school children often underestimate their nasal obstruction. Rhinology 2016;54:164–9.
[4] Kobayashi R, Miyazaki S, Karaki M, et al. Measurement of nasal resistance by rhinomanometry in 892 Japanese elementary school children. Auris Nasus Larynx 2011;38:73–6.
[5] Thulesius HL, Cervin A, Jessen M. The importance of side difference in nasal obstruction and rhinomanometry: a retrospective correlation of symptoms and rhinomanometry in 1000 patients. Clin Otolaryngol 2012;37:17–22.
[6] Chin D, Malek J, Pratt E, Marcells G, Sacks R, Harvey RJ. Patient self-assessment in discriminating the more obstructed side in nasal breathing. J Laryngol Otol 2014;128(Suppl. 1):S34–9.
[7] Mendes AI, Wandalsen GF, Sole D. Objective and subjective assessments of nasal obstruction in children and adolescents with allergic rhinitis. J Pediatr (Rio J) 2012;88:389–95.
[8] Thulesius HL, Cervin A, Jessen M. Can we always trust rhinomanometry? Rhinology 2011;49:46–52.
[9] Julia JC, Burches ME, Martorell A. Active anterior rhinomanometry in paediatrics. Normality criteria. Allergol Immunopathol 2011;39:342–6.
[10] Lin CL, Tawhai MH, McLennan G, Hoffman EA. Computational fluid dynamics. IEEE Eng Med Biol Mag 2009;28:25–33.
[11] Elad D, Liebenthal R, Wenig BL, Einav S. Analysis of air flow patterns in the human nose. Med Biol Eng Comput 1993;31:585–92.
[12] Keyhani K, Scherer PW, Mozell MM. Numerical simulation of airflow in the human nasal cavity. J Biomech Eng 1995;117:429–41.
[13] Wen J, Inthavong K, Tu J, Wang S. Numerical simulations for detailed airflow dynamics in a human nasal cavity. Respir Physiol Neurobiol 2008;161:125–35.
[14] Xiong GX, Zhan JM, Jiang HY, Li JF, Rong LW, Xu G. Computational fluid dynamics simulation of airflow in the normal nasal cavity and paranasal sinuses. Am J Rhinol 2008;22:477–82.
[15] Mosges R, Buchner B, Kleiner M, Freitas R, Horschler I, Schroder W. Computational fluid dynamics analysis of nasal flow. B-ENT 2010;6:161–5.
[16] Kim SK, Na Y, Kim JI, Chung SK. Patient specific CFD models of nasal airflow: overview of methods and challenges. J Biomech 2013;46:299–306.
[17] Wang de Y, Lee HP, Gordon BR. Impacts of fluid dynamics simulation in study of nasal airflow physiology and pathophysiology in realistic human three-dimensional nose models. Clin Exp Otorhinolaryngol 2012;5:181–7.
[18] Li C, Farag AA, Maza G, et al. Investigation of the abnormal nasal aerodynamics and trigeminal functions among empty nose syndrome patients. Int Forum Allergy Rhinol 2017;8:444–52.
[19] Balakin BV, Farbu E, Kosinski P. Aerodynamic evaluation of the empty nose syndrome by means of computational fluid dynamics. Comput Methods Biomech Biomed Eng 2017;20:1554–61.
[20] Chen XB, Lee HP, Chong VF, Wang de Y. Assessment of septal deviation effects on nasal air flow: a computational fluid dynamics model. Laryngoscope 2009;119:1730–6.
[21] Garcia GJ, Rhee JS, Senior BA, Kimbell JS. Septal deviation and nasal resistance: an investigation using virtual surgery and computational fluid dynamics. Am J Rhinol Allergy 2010;24:e46–53.
[22] Segal RA, Kepler GM, Kimbell JS. Effects of differences in nasal anatomy on airflow distribution: a comparison of four individuals at rest. Ann Biomed Eng 2008;36:1870–82.
[23] Chen XB, Leong SC, Lee HP, Chong VF, Wang DY. Aerodynamic effects of inferior turbinate surgery on nasal airflow—A computational fluid dynamics model. Rhinology 2010;48:394–400.

[24] Iwasaki T, Saitoh I, Takemoto Y, et al. Improvement of nasal airway ventilation after rapid maxillary expansion evaluated with computational fluid dynamics. Am J Orthod Dentofacial Orthop 2012;141:269–78.
[25] Spoor CF, Zonneveld FW, Macho GA. Linear measurements of cortical bone and dental enamel by computed tomography: applications and problems. Am J Phys Anthropol 1993;91:469–84.
[26] Fajardo RJ, Ryan TM, Kappelman J. Assessing the accuracy of high-resolution X-ray computed tomography of primate trabecular bone by comparisons with histological sections. Am J Phys Anthropol 2002;118:1–10.
[27] Coleman MN, Colbert MW. Technical note: CT thresholding protocols for taking measurements on three-dimensional models. Am J Phys Anthropol 2007;133:723–5.